The Astrophysical Journal Letters, 902:L25 (7pp), 2020 October 10 https://doi.org/10.3847/2041-8213/abbc20

Exclusion of Cosmic Rays from Molecular Clouds by Self-generated Electric Fields

Kedron Silsbee and Alexei V. Ivlev
Max-Planck-Institut für Extraterrestrische Physik, D-85748 Garching, Germany; ksilsbee@mpe.mpg.de, ivlev@mpe.mpg.de
Received 2020 August 21; revised 2020 September 23; accepted 2020 September 28; published 2020 October 13

Abstract

It was recently discovered that in some regions of the Galaxy, the cosmic-ray (CR) abundance is several orders of magnitude higher than previously thought. Additionally, there is evidence that in molecular cloud envelopes, the CR ionization may be dominated by electrons. We show that for regions with high, electron-dominated ionization, the penetration of CR electrons into molecular clouds is modulated by the electric field that develops as a result of the charge they deposit. We evaluate the significance of this novel mechanism of self-modulation and show that the CR penetration can be reduced by a factor of a few to a few hundred in high-ionization environments, such as those found near the Galactic center.

Unified Astronomy Thesaurus concepts: Galactic cosmic rays (567); Interstellar plasma (851); Interstellar medium (847)

1. Introduction

Understanding the transport of cosmic rays (CRs) in dense gas is one of the big open questions of astrophysics. Low-energy CRs govern the evolution of molecular clouds and the formation of stars (Caselli & Ceccarelli 2012; Padovani et al. 2020), being the dominant source of ionization (McKee 1989; Keto & Caselli 2008; Neufeld & Wolfire 2017) and UV emission (Prasad & Tarafdar 1983) above a column density of $\sim 10^{22}$ cm^{-2}. These processes affect both the chemistry (Keto & Caselli 2008; Keto et al. 2014) and thermodynamics (Galli et al. 2002; Glassgold et al. 2012; Ivlev et al. 2019) of the clouds. Furthermore, the level of ionization governs the degree to which the gas is coupled to the magnetic field (Shu et al. 1987). This has profound implications for the existence and size of disks around young stars (Zhao et al. 2016, 2018).

For a long time the CR ionization rate ζ was thought to likely be on the order of 10^{-17} s^{-1}, based on measurements of the CR abundance near Earth (Spitzer & Tomasko 1968). More recently there have been measurements of ζ in nearby molecular clouds (Indriolo & McCall 2012), suggesting ζ as high as 10^{-15} s^{-1} toward some clouds. In some environments the CR ionization rates can be orders of magnitude higher still. In the Central Molecular Zone (CMZ) of the Galaxy, Le Petit et al. (2016) and Oka et al. (2019) estimate ζ of 1–11 $\times$ 10^{-14} s^{-1} and 2 $\times$ 10^{-14} s^{-1}, respectively. Yusef-Zadeh et al. (2007) suggest a rate of 5 $\times$ 10^{-13} s^{-1} in the Sagittarius C region. There is also evidence of extremely high CR abundance near young stars (Ainsworth et al. 2014; Ceccarelli et al. 2014).

It is not known whether CR protons or electrons are the primary source of ionization. As shown in Padovani et al. (2018), if the spectra of electrons and protons measured by the Voyager probes (Stone et al. 2019) are extrapolated down to lower energies, then ζ is dominated by electrons at column densities lower than 2 $\times$ 10^{21} cm^{-2}. If the CR electron and proton spectra have the slope appropriate for acceleration in strong shocks, then ionization is dominated by electrons unless protons dominate the total CR energy by factors of tens.

The commonly used free-streaming model for the CR transport in clouds and disks (Padovani et al. 2009, 2018) holds that they propagate along local magnetic field lines without substantial pitch-angle scattering, and lose energy due to interactions with the gas in the cloud (losses are dominated by ionization for nonrelativistic particles). The fundamental effect completely neglected in such models (also those including CR scattering on magnetic disturbances) is an inevitable net deposition of charge within the cloud. Low-energy CRs are absorbed in the cloud, becoming thermalized charged particles. So as to maintain charge balance within the cloud, the thermal plasma must transport a net current. Because the plasma has a finite conductivity, this implies the presence of a long-range electric field, which acts to modulate the penetration of CRs.

This mechanism of CR modulation—which has not been considered thus far, to our knowledge—is the topic of the present Letter. We show that the self-generated electric field is strong enough to have a large effect for reasonable parameters, provided CR electrons dominate the ionization.

2. Linear Regime

Let us calculate the steady-state electric potential in a cloud in the limit that the incoming CR flux is not modulated by the electric field. We approximate the cloud as a slab of a weakly ionized cool gas with uniform density n, embedded in a warm infinitely conducting medium filled with CRs. The magnetic field lines are assumed to be straight, but may enter the cloud at an arbitrary angle with respect to the surface. The column density N relevant to the CR propagation is defined by integrating the density *along the magnetic field*. The distance z is measured in this direction, too, and set to 0 at the cloud center, where N is half of the total cloud value $N_{\rm cl}$. For typical diffuse clouds (even with the extreme ionization implied by our model), the plasma conductivity parallel to the magnetic field is higher by at least 6 orders of magnitude than the perpendicular conductivity. Hence, the current due to charge deposition by CRs in the region between 0 and z within the cloud must be simply balanced by the parallel plasma current at position z.

Keeping in mind that the cloud is bombarded by CRs from both sides, the CR current $J_{\rm CR}$ at column N is given by the integral

$$J_{\rm CR}(N) = 2\pi q_{\rm CR} \int_0^1 d\mu\ \mu \int_{\mathscr{E}_{\rm ext}(N/\mu)}^{\mathscr{E}_{\rm ext}([N_{\rm cl}-N]/\mu)} d\mathscr{E}\ j_i(\mathscr{E}), \qquad (1)$$

where $q_{\rm CR} = \pm e$ is the charge of a CR particle and μ is the cosine of the pitch angle. The integration limits are determined by the extinction energy $\mathscr{E}_{\rm ext}(N)$—the lowest energy of a particle that can penetrate to column depth N. The external (initial) spectrum of CRs, $j_i(\mathscr{E})$, is assumed to be isotropic and given by

$$j_i(\mathscr{E}) = j_0\left(\frac{\mathscr{E}_0}{\mathscr{E}}\right)^a \ {\rm s^{-1}\,cm^{-2}\,eV^{-1}\,sr^{-1}}. \tag{2}$$

To determine $\mathscr{E}_{\rm ext}(N)$, we must introduce the ionization loss function. This is given in Padovani et al. (2018) as

$$L \equiv \frac{d\mathscr{E}}{dN} = L_0\left(\frac{\mathscr{E}_0}{\mathscr{E}}\right)^s, \tag{3}$$

and then

$$\mathscr{E}_{\rm ext}(N) = \mathscr{E}_0\left(\frac{N}{N_0}\right)^{\frac{1}{1+s}}, \tag{4}$$

where $N_0 = (1+s)^{-1}\mathscr{E}_0/L_0$. Performing the integral in Equation (1) yields

$$J_{\rm CR}(N) = \frac{2\pi(1+s)q_{\rm CR}j_0\mathscr{E}_0}{(1-a)(1+2s+a)}\left[(\tilde{N}_{\rm cl}-\tilde{N})^{\frac{1-a}{1+s}} - \tilde{N}^{\frac{1-a}{1+s}}\right], \tag{5}$$

where $\tilde{N} \equiv N/N_0$. For $a = 1$,

$$J_{\rm CR}(N) = \frac{\pi q_{\rm CR}j_0\mathscr{E}_0}{1+s}\ln\left(\frac{N_{\rm cl}-N}{N}\right). \tag{6}$$

If we are interested in column densities between 10^{19} and $10^{22}\,{\rm cm^{-2}}$, the relevant energies are from 5 to 300 KeV for electrons, and from 100 KeV to 8 MeV for protons. The loss functions on these intervals are well approximated by Equation (3) with $s = 0.75$, $L_0 = 2.0\times10^{-16}$ eV cm^2, $\mathscr{E}_0 = 10$ KeV for electrons, and $s = 0.78$, $L_0 = 3.7\times10^{-16}$ eV cm^2, $\mathscr{E}_0 = 10$ MeV for protons. Even though s may change a little, depending on the energy range, these variations have negligible impact on our results. Therefore, in this Letter we employ the above values for numerical calculations, while keeping s explicitly in the analytical results. As in Padovani et al. (2018), we use the number density of all gas particles, rather than of hydrogen atoms, and assume the hydrogen to be molecular.

Let us denote with E the electric field component *parallel* to the magnetic field. The value of $E(N)$ in the cloud is obtained from the the steady-state condition

$$J_{\rm CR}(N) + J_{\rm pl}(E) = 0, \tag{7}$$

where $J_{\rm pl} = \sigma E$ is the plasma current along the magnetic field, determined by the corresponding electric conductivity (Braginskii 1965),

$$\sigma = 5\times10^9\ {\rm s^{-1}}\left(\frac{T}{50\ {\rm K}}\right)^{3/2}. \tag{8}$$

Equation (8) assumes a fully ionized plasma. The expected ionization fraction in the outer layers of a cloud is in excess of 10^{-3} (Neufeld & Wolfire 2017). Since the electron–neutral collision cross section is lower by 5 or 6 orders of magnitude than the electron–ion cross section for such conditions, the neutrals have a negligible effect on the parallel conductivity.

Consider the CR spectra measured from the Voyager probes (Stone et al. 2019) and extrapolated to lower energies as in Padovani et al. (2018), and a cloud with $N_{\rm cl} = 6\times10^{21}\,{\rm cm^{-2}}$, $n = 60\,{\rm cm^{-3}}$, and $T = 50$ K (Draine 2011). From Equations (5), (7), and (8) we derive the magnitude of the electric potential energy $e|\phi(N)|$ for CR protons (p) and electrons (e), and compare these with the respective extinction energies $\mathscr{E}_{\rm ext}(N)$. We obtain that $e\phi_p$ is completely negligible at any N, while $e|\phi_e(N)|$ is just a factor of 30 less than $\mathscr{E}_{{\rm ext},e}(N)$. Since the electron spectrum dominates the ionization at low column density, this implies that if the CR abundance were increased by a factor of 30, then ζ would be significantly affected by the electron charge buildup. Such an increased spectrum would result in a total ionization rate of somewhat less than $10^{-15}\ {\rm s^{-1}}$ at a column density of $10^{21}\ {\rm cm^{-2}}$. This value is within the range estimates made by Indriolo & McCall (2012), suggesting that this effect may play a role, even in local molecular clouds.

The importance of the electric field (at a given ζ) is substantially higher if the ionization is dominated by electrons. Consider locations adjacent to a strong shock that is acting as a source of CRs, so one can expect $\mathscr{F}(p) \propto p^{-2}$ for the particle density in *momentum space*. Assuming an electron-to-proton ratio of χ, and column densities such that the ionization is dominated by nonrelativistic particles (up to a few times $10^{22}\,{\rm cm^{-2}}$ for electrons, and a few times $10^{25}\,{\rm cm^{-2}}$ for protons), we obtain the *energy* spectra given by Equation (2) with $j_{0,e}/j_{0,p} = \chi m_p/m_e$. Then Equation (6) shows that the deposited charge is dominated by electrons if $\chi > m_e/m_p$. From Equation (31) of Silsbee & Ivlev (2019), we find that the ratio of the ionization rates at a given column density is $\zeta_e/\zeta_p \sim \chi(m_p/m_e)^{s/(1+s)}$ (for simplicity, we assume the same s for electrons and ions and set $L_{0,e}/L_{0,p} \sim m_e/m_p$). From this we conclude that, if χ is greater than a few percent, then both the ionization and the charge deposition are dominated by electrons.

Studies of particle acceleration are still uncertain as to the value of χ—there is evidence that it is less than 1% in quasi-parallel shocks (Park et al. 2015). On the other hand, there is recent evidence (Spitkovsky et al. 2019) that quasi-perpendicular shocks in fact preferentially accelerate electrons. Hence, it is reasonable to assume that there are regions where more than a few percent of the electrons have been produced in quasi-perpendicular shocks, and therefore for the remainder of this Letter, we consider regions in which CR electrons dominate the ionization rate.

3. High-flux Limit for CR Electrons

We now approach the problem from a different perspective. Instead of assuming the electric field to be a small perturbation on the propagation of CRs, we consider it to be the dominant effect and treat ionization losses as a perturbation. To be more precise, we assume that at every position of interest within the cloud, the electric potential ϕ satisfies $e|\phi| \gg \mathscr{E}_{\rm ext}$.

Let us consider, as before, a slab of uniform gas with a constant angle between the magnetic field and the surface. Now the distance coordinate z, measured along the magnetic field, is set to be 0 at one edge of the cloud. We posit that the absolute value of the potential as a function of z over some range of

distances is given by

$$|\phi(z)| = \frac{\mathscr{E}_0}{e}\left(\frac{z}{z_0}\right)^f, \tag{9}$$

with the length scale z_0 and exponent $0 < f < 1$ to be determined. Obviously since the electric field changes direction at the center of the cloud, this form for $\phi(z)$ is not valid near the center of the cloud, so we restrict our attention to z much smaller than the cloud size. This allows us to solve for E, the electric field component parallel to the magnetic field, as a function of position:

$$E(z) = E_0\left(\frac{z}{z_0}\right)^{f-1}, \tag{10}$$

where $E_0 = f\mathscr{E}_0/(ez_0)$.

Instead of using variables $\mathscr{E}$ and μ for our problem below we find it more convenient to work with the "parallel" and "perpendicular" energies $\mathscr{E}_\parallel = \mathscr{E}\mu^2$ and $\mathscr{E}_\perp = \mathscr{E}(1-\mu^2)$. The local spectrum per unit $\mathscr{E}_\parallel$ and $\mathscr{E}_\perp$ can be conveniently calculated from the local density in the momentum space. According to the Liouville theorem, the CR density in momentum space is conserved along the phase trajectories, that is to say $\mathscr{F}(\boldsymbol{p}, \boldsymbol{r}) = \mathscr{F}_i(p^2 + 2me|\phi(r)|)$. Combining this with a general relation $j(\mathscr{E}, \mu) = p^2\mathscr{F}(p, \mu)$, we find $\mathscr{F}(p, z) = j_i(\mathscr{E} + e|\phi|)/[2m(\mathscr{E} + e|\phi|)]$. Then, noting that $2\pi p_\perp dp_\perp dp_\parallel = \pi m\sqrt{2m/\mathscr{E}_\parallel}\, d\mathscr{E}_\parallel d\mathscr{E}_\perp$, we multiply $\mathscr{F}(p, z)$ with the physical velocity $\sqrt{2\mathscr{E}/m}$ and the pre-factor $\pi m\sqrt{2m/\mathscr{E}_\parallel}$, which yields the spectrum expressed in new variables,

$$j(\mathscr{E}_\parallel, \mathscr{E}_\perp, z) = \pi\sqrt{\frac{\mathscr{E}}{\mathscr{E}_\parallel}}\,\frac{j_i(\mathscr{E} + e|\phi|)}{(\mathscr{E} + e|\phi|)}, \tag{11}$$

where we use $\mathscr{E} = \mathscr{E}_\parallel + \mathscr{E}_\perp$ for brevity.

As the first step, we equate the current of CRs that are absorbed beyond position z due to the losses and the plasma current along the magnetic field. Integrating over the *initial* CR distribution at the cloud edge, we obtain

$$\frac{\sigma E(z)}{e} = \int_{e|\phi(z)|}^{\infty} d\mathscr{E}_\parallel \int_0^{\mathscr{E}_\perp^{\rm cr}(\mathscr{E}_\parallel)} d\mathscr{E}_\perp\, j(\mathscr{E}_\parallel, \mathscr{E}_\perp, 0), \tag{12}$$

with σ from Equation (8). Particles with $\mathscr{E}_\perp = 0$ will have zero kinetic energy at the turning point, and will therefore be stopped and contribute to the charge buildup. Particles with relatively large $\mathscr{E}_\perp$ have enough transverse energy that they are accelerated back to the cloud edge before their energy is damped. Hence, for particles with a given $\mathscr{E}_\parallel$ there is a critical value of $\mathscr{E}_\perp$, denoted $\mathscr{E}_\perp^{\rm cr}$, which determines their trapping inside the cloud. As discussed in Appendix A, the dynamics of a particle with initial transverse energy $\mathscr{E}_\perp$ in the presence of losses are determined by a dimensionless number

$$M = \frac{eE_{\rm turn}}{nL(\mathscr{E}_\perp)}, \tag{13}$$

where $E_{\rm turn}$ is the parallel electric field at the turning point. The critical initial transverse energy $\mathscr{E}_\perp^{\rm cr}$ for $\mathscr{E}_\parallel = e|\phi(z)|$ corresponds to $M_{\rm cr} \approx 3.6$: for $M < M_{\rm cr}$, particles are stopped by the losses near the turning point; otherwise, they return back to the cloud edge. Using Equations (9) and (10), we find that the electric field at the turning point is

$$E_{\rm turn} = E_0\left(\frac{\mathscr{E}_0}{\mathscr{E}_\parallel}\right)^{\frac{1-f}{f}}. \tag{14}$$

Combining Equations (13) and (14), we find

$$\mathscr{E}_\perp^{\rm cr} = \mathscr{E}_0\left(M_{\rm cr}\frac{nL_0}{eE_0}\right)^{\frac{1}{s}}\left(\frac{\mathscr{E}_\parallel}{\mathscr{E}_0}\right)^{\frac{1-f}{sf}}. \tag{15}$$

Plugging Equation (15) into (12) and approximating that $\mathscr{E}_\perp^{\rm cr} \ll \mathscr{E}_\parallel$ (which is verified in Section 3.2), we can evaluate the integral in Equation (12) under condition $f(1+as) > 1$. This yields

$$\frac{\sigma E_0}{e}\left(\frac{z_0}{z}\right)^{1-f} = \pi j_0\mathscr{E}_0\left(M_{\rm cr}\frac{nL_0}{eE_0}\right)^{\frac{1}{s}} \times \frac{sf}{f(1+as)-1}\left(\frac{z_0}{z}\right)^{\frac{f(1+as)-1}{s}}. \tag{16}$$

Matching powers of z, we find

$$f = \frac{1+s}{1+s+as}. \tag{17}$$

This allows us to solve for z_0:

$$\frac{nz_0}{N_0} = \left(\frac{(1+s)^{\frac{1}{s}-1}f^{\frac{1}{s}+1}}{M_{\rm cr}^{\frac{1}{s}}}\,\frac{as\sigma n}{\pi e^2 j_0 N_0}\right)^{\frac{s}{1+s}}. \tag{18}$$

We note that the condition $f(1+as) > 1$ is reduced to $a > 0$. We finally derive

$$\frac{e|\phi|}{\mathscr{E}_{\rm ext}} = \left(\frac{N_0}{nz_0}\right)^{\frac{1+s}{1+s+as}}\left(\frac{N}{N_0}\right)^{\frac{s(1+s-a)}{(1+s)(1+s+as)}}, \tag{19}$$

naturally, invariant with respect to the choice of $\mathscr{E}_0$. We require $e|\phi|/\mathscr{E}_{\rm ext} \gg 1$ in order for the solution in Equation (19) to be valid. Formally, it must break down either at high or low N, depending on the sign of the slope. In fact, however, the slope is very small: ≈ 0.13 (-0.03) for $a = 1$ $(a = 2)$. For this reason, as a practical matter, over the range of column density of interest the solution either applies everywhere, or applies nowhere—depending on the magnitude of nz_0/N_0, which is the chief parameter characterizing the effect of self-generated field.

Now we can calculate the ionization rate in the high-flux limit. Again, we assume that the regular (ionization) losses play no role in determining the local CR spectrum, which is determined purely by the external spectrum and the electric potential. The primary CR ionization rate of H_2 at position z is given by

$$\zeta_\phi(z) = \frac{2}{\epsilon}\int_0^\infty\int_0^\infty d\mathscr{E}_\parallel d\mathscr{E}_\perp j(\mathscr{E}_\parallel, \mathscr{E}_\perp, z)L(\mathscr{E}), \tag{20}$$

where $j(\mathscr{E}_\parallel, \mathscr{E}_\perp, z)$ is given by Equation (11) and ϵ is the mean energy lost per primary ionization event (Silsbee & Ivlev 2019), which we take to be 58 eV. We obtain

$$\zeta_\phi = \frac{4\pi B j_0 L_0\mathscr{E}_0}{\epsilon}\left(\frac{e|\phi|}{\mathscr{E}_0}\right)^{-(a+s-1)}, \tag{21}$$

where $B \equiv B(2-s,\ a+s-1)$ is the beta function (see Appendix B). By comparing Equation (21) with Equation (31) of Silsbee & Ivlev (2019), which describes the "regular" CR ionization rate $\zeta(N)$, we obtain

$$\frac{\zeta_\phi}{\zeta} \approx 1.7\left(\frac{e|\phi|}{\mathscr{E}_{\rm ext}}\right)^{-(a+s-1)}, \tag{22}$$

where $e|\phi|/\mathscr{E}_{\rm ext}$ is given by Equation (19) and the pre-factor is accurate within 3% for $1 \leqslant a \leqslant 2$; see Equation (B3).

We point out that the sign of $a+s-1$ in Equations (21) and (22) coincides with the sign of the exponent that determines the regular dependence $\zeta(N)$; see Equation (33) of Silsbee & Ivlev (2019). In case $a+s-1<0$ the CR spectrum is too hard and low-energy particles are no longer dominating ionization. Hence, as for the case of regular ionization, $a+s-1>0$ is assumed.

3.1. Magnitude of the Effect

Using Equations (3), (8), and (21), we rewrite Equation (19) in terms of the physical parameters:

$$\frac{e|\phi|}{\mathscr{E}_{\rm ext}} \approx 1.3\ \exp(0.35a)\ T_{250}^{-0.58}\ N_{21}^{0.33}\ (\zeta_{-15}/n_{30})^{0.39}, \tag{23}$$

with T_{250} in units of 250 K, N_{21} in units of 10^{21} cm^{-2}, ζ_{-15} (evaluated at same column density) in units of 10^{-15} s^{-1}, and n_{30} in units of 30 cm^{-3}. Equation (23) is accurate to within 2.5% for $1 \leqslant a \leqslant 2$.

As an example, we consider conditions appropriate for the high-ionization rate regions near the Galactic center. We assume that these ionization rates are dominated by CR electrons, and consider an electron spectrum with $a=1$ (appropriate for acceleration by strong shocks) and $a=2$ (for weaker shocks with compression ratio of 2) (Blandford & Ostriker 1978). In both cases, we choose j_0 so that (with the electric field included) the primary ionization rate at $N = 10^{21}$ cm^{-2} is equal to 4×10^{-14} s^{-1}, based on the values of 1–11 $\times 10^{-14}$ s^{-1} reported in Le Petit et al. (2016) for the CMZ.

The top panel of Figure 1 shows a comparison of $e|\phi(N)|$ with $\mathscr{E}_{\rm ext}(N)$. We use $T=250$ K and $n=30$ cm^{-3}, based on the observations in Le Petit et al. (2016). The bottom panel shows a comparison of the ionization rate calculated from Equation (21) with that calculated ignoring electric fields (Equation (31) of Silsbee & Ivlev 2019). At a representative column density of 10^{21} cm^{-2}, $e|\phi|/\mathscr{E}_{\rm ext} \approx 8$ for the spectrum with $a=1$, and ≈11 for $a=2$, leading to reductions in the ionization rate by factors of about 2.7 and 40, respectively. Note that for $T \approx 50$ K, suggested by Figure 9 of Bisbas et al. (2015) for our values of ζ, the reduction would be about 5.3 and 200, respectively.

Limits of the nonrelativistic formulation are reached at higher column densities, where $e|\phi| \gtrsim mc^2$. In Appendix C, the calculations presented in Equations (11)–(19) are redone in the ultrarelativistic regime, assuming that outside the cloud the CR density in momentum space has the same power-law slope for both relativistic and nonrelativistic particles. It is also assumed that the critical kinetic energy is still nonrelativistic near the turning point—this premise is shown to be valid for N substantially higher than 10^{22} cm^{-2}, i.e., well applicable for molecular clouds. We find that the electric potential (19) is

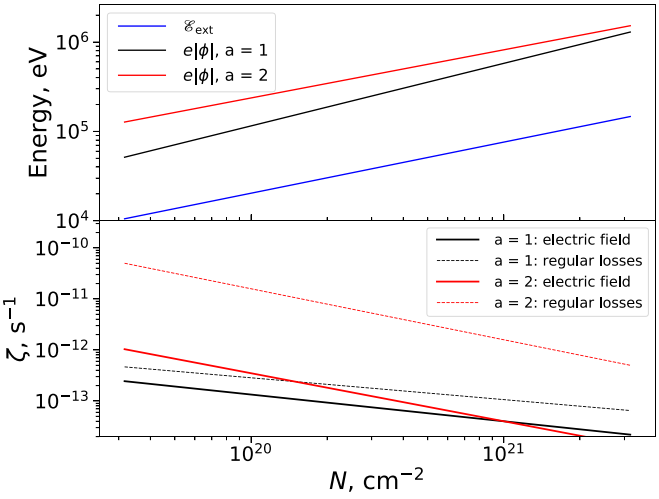

Figure 1. The top panel shows a comparison between the electric energy $e|\phi|$ (Equation (19)) and the extinction energy $\mathscr{E}_{\rm ext}$ (Equation (4)) for CR electrons. The black and red curves are for an electron spectrum with $a=1$ and 2, respectively (normalized such that $\zeta = 4\times10^{-14}$ at $N=10^{21}$ cm^{-2}). The bottom panel shows the corresponding ionization rate, plotted without and with taking into account the self-generated electric field (Equation (31) of Silsbee & Ivlev 2019 and Equation (21) of this Letter, respectively).

modified in the ultrarelativistic regime as

$$\phi_{\rm rel}(N) = \phi(N)\left(\frac{N}{N_{\rm rel}}\right)^{-\frac{s(1+a)(1+s)}{(1+s+as)(1+2s+2as)}}. \tag{24}$$

Here $N_{\rm rel}$ is the column density at which $e|\phi(N)|$ from Equation (19) is equal to $\approx 2.4mc^2$; see Equation (C6). For Figure 1, $N_{\rm rel} = 2$–3×10^{21} cm^{-2} and the exponent varies between −0.26 and −0.22 for $1 \leqslant a \leqslant 2$. Hence, relativistic effects only lead to a minor modification of the self-generated electric field, and the CR modulation remains essentially unchanged.

3.2. Notes on the Derived Solution

Here we verify important assumptions made to derive the above results, and briefly discuss some immediate implications.

3.2.1. Anisotropy

We can check the assumption made after Equation (15), that $\mathscr{E}_\perp^{\rm cr} \ll \mathscr{E}_\parallel$. Setting $e|\phi| \approx \mathscr{E}_\parallel$, we rewrite Equation (15) as

$$\frac{\mathscr{E}_\perp^{\rm cr}}{\mathscr{E}_\parallel} \approx \left(\frac{M_{\rm cr}}{f(1+s)}\right)^{\frac{1}{s}}\left(\frac{\mathscr{E}_{\rm ext}}{e|\phi|}\right)^{\frac{1}{s}+1}. \tag{25}$$

For the parameters in Figure 1, the anisotropy due to CR deposition is expected to be less than a few percent. This means that the excitation of the streaming instability by penetrating CRs will be suppressed compared to a case of no electric field (Morlino & Gabici 2015; Ivlev et al. 2018; where the pitch-angle anisotropy could be of order unity).

3.2.2. Electric Fields from Alfvén Waves

We have implicitly assumed that the deposition of CRs is the only source of a large-scale electric field parallel to the magnetic field. In fact, an electric field could also be produced by Alfvén waves present in the cloud as a result of turbulence.

In ideal MHD, such fields are perpendicular to the local magnetic field, and thus do no work on CRs. It is worth noting though that the strength of this electric field, associated with turbulent motions with the velocity u, is on the order of $uB/c \sim 10^{-11}$ statV cm^{-1} for typical parameters. This is $\sim 10^5$ times stronger than the field from the modulation effect, and therefore it could be significant if there were even a very small deviation from orthogonality.

In particular, Bian et al. (2010) and Klimushkin & Mager (2014) suggest that under realistic conditions, Alfvén waves are able to generate a small parallel electric field, but its strength is highly uncertain. The authors developed a model under which the ratio of parallel to perpendicular electric field is roughly the squared ratio of the ion gyroradius to the wavelength. Estimates of the lower wavelength bound for Alfvén waves, given in Appendix C of Kulsrud & Pearce (1969), suggest that waves are cut off around the ambipolar damping scale of $\sim 10^{16}$ cm for our conditions. For typical magnetic fields, the ion gyroradius is a few times 10^6 cm, so the parallel electric field arising from such a mechanism is smaller than the perpendicular field by some 19 orders of magnitude.

We are not aware of a model that shows a significant parallel electric field in the long-wavelength limit. However, as both the cutoff scale of Alfvén waves and the magnitude of parallel electric field are subject to significant uncertainties, this could be an interesting avenue of future work.

3.2.3. Joule Heating

The electric current $J_{\rm pl} = \sigma E$ induced in the gas due to CR deposition represents an additional source of gas heating. The rate of the resulting Joule heating is

$$H_J = \sigma E^2. \tag{26}$$

This should be compared to the rate of regular gas heating by CRs, given by

$$H_{\rm CR} = \eta \epsilon \zeta_\phi n, \tag{27}$$

where η is an efficiency factor of order 40% (Glassgold et al. 2012). As shown in Appendix D, their ratio is

$$\frac{H_J}{H_{\rm CR}} = Q\left(\frac{e|\phi|}{\mathscr{E}_{\rm ext}}\right)^{-\frac{1}{s}+s}, \tag{28}$$

where Q varies between ≈ 7 and ≈ 10 for $1 \leqslant a \leqslant 2$. Thus, for conditions illustrated in Figure 1, Joule heating is larger than the regular CR heating by a factor that varies monotonically between 2.0 and 2.4 for $1 \leqslant a \leqslant 2$. Regardless of a, Joule heating becomes subdominant in the limit of very strong self-modulation.

4. Conclusion

We propose a novel mechanism of CR self-modulation, which can substantially reduce the penetration of CR electrons into molecular clouds. The penetration is limited by the electric fields generated due to the deposition of those same electrons. If the electron spectrum is produced by acceleration in strong shocks, the ionization rate can be reduced by a factor of a few in the high-ionization environments found in our Galaxy, such as the CMZ. The reduction becomes much stronger for steeper spectra, appropriate for weaker shocks. Hence, the high-ionization rates near the Galactic center could imply even higher CR energy densities than previously thought. The effect is more pronounced at lower gas number densities, where direct measurements of the ionization can be made. The ionization rate in denser regions will therefore be much higher than would be predicted from measurements coupled with conventional models of CR transport. Furthermore, the electric current induced in the gas due to the CR deposition represents an additional heating source. We show that the resulting Joule heating could be of similar magnitude to the regular gas heating by CRs.

Appendix A
Calculation of $\mathscr{E}_\perp^{\rm cr}(\mathscr{E}_\parallel)$

As stated in the main text, we consider the limit $e|\phi| \gg \mathscr{E}_{\rm ext}$. In this case only particles with sufficiently small $\mathscr{E}_\perp$ can be trapped in a cloud, as they are slowed nearly to a stop at the turning point, thus suffering strong ionization losses. To estimate $\mathscr{E}_\perp^{\rm cr}(\mathscr{E})$, we use the loss function given by Equation (3). We are dealing with nonrelativistic particles, such that their velocities are $v = \sqrt{2\mathscr{E}/m}$, where m is the particle mass.

We note that for a particle moving parallel to an electric field with strength E, there is a critical energy $\mathscr{E}_{\rm cr}$ such that the drag force $nL(\mathscr{E}_{\rm cr})$ due to energy losses is compensated by the acceleration from the electric field,

$$\mathscr{E}_{\rm cr} = \mathscr{E}_0\left(\frac{nL_0}{eE}\right)^{\frac{1}{s}}. \tag{A1}$$

We assume that if $\mathscr{E}_{\rm cr}$ is reached after turnaround, this occurs in a short distance from the turning point, and we can therefore calculate $\mathscr{E}_\perp^{\rm cr}$ assuming a constant electric field. This assumption is verified at the end of our calculation.

In a constant electric field E, the equations of motion for the parallel and transverse velocities are

$$m\dot{v}_\parallel = -eE - nL(\mathscr{E})\frac{v_\parallel}{v}, \qquad m\dot{v}_\perp = -nL(\mathscr{E})\frac{v_\perp}{v}. \tag{A2}$$

Normalizing the velocity to the initial transverse velocity, $\tilde{v} = v/v_{\perp i}$, and time to

$$\tau = \frac{mv_{\perp i}}{nL(\mathscr{E}_{\perp i})}, \tag{A3}$$

we then arrive at the equations

$$\dot{\tilde{v}}_\parallel = -M - \tilde{v}_\parallel \tilde{v}^{-2s-1}, \qquad \dot{\tilde{v}}_\perp = -\tilde{v}_\perp \tilde{v}^{-2s-1}, \tag{A4}$$

containing a single dimensionless number

$$M = \frac{eE}{nL(\mathscr{E}_{\perp i})}. \tag{A5}$$

To distinguish between the local and initial values, here we identify the latter with the subscript i. The numerical solution of Equations (A4) shows that for $M < M_{\rm cr} \approx 3.6$ particle trajectories decay to zero velocity. Furthermore, we find that for $M/M_{\rm cr} \leqslant 0.999$, the final position of the particle relative to the turning point $z_{\rm turn}$ satisfies $\Delta z < 0.2\, v_{\perp i}\tau = 0.4M\, \mathscr{E}_{\perp i}/(eE)$. Noting that the turning point occurs approximately where $e|\phi(z)| = \mathscr{E}_{\parallel i}$ and using Equations (9) and (10) we find

$z_{\rm turn} = f\mathscr{E}_{\parallel i}/(eE)$, and

$$\frac{\Delta z}{z_{\rm turn}} < \frac{0.4M}{f}\frac{\mathscr{E}_{\perp i}}{\mathscr{E}_{\parallel i}}. \tag{A6}$$

As shown in Equation (25), in the limit $e|\phi| \gg \mathscr{E}_{\rm ext}$ we have $\mathscr{E}_\perp^{\rm cr}/\mathscr{E}_\parallel \ll 1$ and, hence, $\Delta z/z_{\rm turn} \ll 1$. Thus, the assumption that trapped particles are stopped near the turning point is justified.

Appendix B
Derivation of Equations (21) and (22)

We substitute $L(\mathscr{E})$ and $j(\mathscr{E}_\parallel, \mathscr{E}_\perp, z)$, given by Equations (3) and (11) to (20) and, normalizing energies by $e|\phi|$, readily obtain Equation (21) with the pre-factor proportional to the following double integral:

$$I(a, s) = \int_0^\infty \int_0^\infty dpdq\ \frac{(p+q)^{1/2-s}}{\sqrt{p}\,(p+q+1)^{a+1}}. \tag{B1}$$

We replace the integration variables p, q by x^2, y^2 and rewrite the integral in polar coordinates with $r = \sqrt{x^2+y^2}$ and $\tan\theta = y/x$. Integrating over θ between 0 and $\pi/2$ and then substituting $r = \sqrt{t/(1-t)}$ yields

$$I(a, s) = 2B(2-s, a+s-1), \tag{B2}$$

expressed via the beta function.

Equation (22) is derived by comparing Equation (21) with Equation (31) of Silsbee & Ivlev (2019), which describes the "regular" CR ionization rate $\zeta(N)$. We note that Equation (31) should be multiplied by 2π, due to a different normalization of the CR spectrum in Silsbee & Ivlev (2019), and d denotes s in our Letter. Also, unlike Silsbee & Ivlev (2019), we assume that the magnetic field has constant strength, so there is no magnetic mirroring (Silsbee et al. 2018). The integral I_f, entering Equations (31) and given by Equation (32) of Silsbee & Ivlev (2019), can also be expressed via the beta function, by substituting $x^{1+s} = t/(1-t)$ for the integration variable. Using Equation (4), we finally obtain

$$\frac{\zeta_\phi}{\zeta} = 2(a+2s)\,\frac{B(2-s, a+s-1)}{B\left(\frac{1}{1+s}, \frac{a+s-1}{1+s}\right)}\left(\frac{e|\phi|}{\mathscr{E}_{\rm ext}}\right)^{-(a+s-1)}. \tag{B3}$$

The pre-factor of $(e|\phi|/\mathscr{E}_{\rm ext})$ is a slowly varying function of a, equal to ≈ 1.7 for $1 \leqslant a \leqslant 2$.

Appendix C
The Ultrarelativistic Regime

We calculate the electric potential in the limit $e|\phi| \gg mc^2$, assuming that the kinetic energy at the turning point is still less than mc^2, so the loss function of Equation (3) can be used.

Consider interstellar CRs with the density in momentum space having the same power-law slope for both relativistic and nonrelativistic energies. The corresponding kinetic energy spectrum reads

$$j_i(\mathscr{E}) = j_0\left(\frac{2mc^2\mathscr{E}_0}{\mathscr{E}^2 + 2mc^2\mathscr{E}}\right)^a. \tag{C1}$$

For nonrelativistic particles, Equation (C1) is reduced to the spectrum of Equation (2), adopted in the main text. In the ultrarelativistic regime, the spectrum becomes $j_i(\mathscr{E}) = j_{0,\rm rel}(\mathscr{E}_0/\mathscr{E})^{2a}$ with $j_{0,\rm rel} = (2mc^2/\mathscr{E}_0)^a j_0$. This allows us to easily extend our calculations to the ultrarelativistic case.

Following the same logic as in the main text, but using $\mathscr{E} = pc$ instead of $\mathscr{E} = p^2/(2m)$, we find

$$j(\mathscr{E}_\parallel, \mathscr{E}_\perp, z) = 2\pi\mathscr{E}_\perp\frac{j_i(\mathscr{E} + e|\phi|)}{(\mathscr{E} + e|\phi|)^2}, \tag{C2}$$

with $\mathscr{E} = \sqrt{\mathscr{E}_\parallel^2 + \mathscr{E}_\perp^2}$, in lieu of Equation (11). While Equation (12) remains unchanged, the calculation of the initial $\mathscr{E}_\perp^{\rm cr}$ proceeds differently. We assume that the critical energy *near the turning point* is nonrelativistic. Then its value is still given by Equation (15). Next, we note that the perpendicular momentum $p_\perp$ is a conserved quantity (neglecting losses). Setting $p_\perp^2/(2m)$ at the turning point equal to the right-hand side of Equation (15), we find the critical value of the *initial* transverse energy $\mathscr{E}_\perp = cp_\perp$,

$$\mathscr{E}_\perp^{\rm cr} = \sqrt{2mc^2\mathscr{E}_0}\left(M_{\rm cr}\frac{nL_0}{eE_0}\right)^{\frac{1}{2s}}\left(\frac{\mathscr{E}_\parallel}{\mathscr{E}_0}\right)^{\frac{1-f_{\rm rel}}{2sf_{\rm rel}}}, \tag{C3}$$

to be substituted in Equation (12). As before, we approximate $\mathscr{E}_\perp^{\rm cr} \ll \mathscr{E}_\parallel$ and obtain an equation analogous to Equation (16), which yields

$$f_{\rm rel} = \frac{1+s}{1+2s+2as}, \tag{C4}$$

and

$$\frac{nz_{0,\rm rel}}{N_0} = \left[\frac{(1+s)^{\frac{1}{s}-1}f_{\rm rel}^{\frac{1}{s}+1}}{M_{\rm cr}^{\frac{1}{s}}}\frac{2as\sigma n}{\pi e^2 j_{0,\rm rel}N_0}\left(\frac{\mathscr{E}_0}{2mc^2}\right)\right]^{\frac{s}{1+s}}. \tag{C5}$$

Equation (C5) is similar to Equation (18) where parameters a, f, and j_0 are replaced with the respective ultrarelativistic values, and the extra factor $\mathscr{E}_0/(2mc^2)$ originates from the square-root factor in Equation (C3).

Using Equation (C5), we obtain an ultrarelativistic relation $e|\phi|_{\rm rel}/\mathscr{E}_{\rm ext}$ versus N. By comparing this with the nonrelativistic relation, Equation (19), we derive Equation (24) where $N_{\rm rel}$ is the column such that

$$\frac{e|\phi(N_{\rm rel})|}{mc^2} = 2\left[\frac{1}{2}\left(\frac{1+2s+2as}{1+s+as}\right)^{\frac{1}{s}+1}\right]^{\frac{1}{1+a}} \equiv \psi(a, s). \tag{C6}$$

For $1 \leqslant a \leqslant 2$, we have $\psi(a, s) \approx 2.4$.

Finally, we verify the assumption made in the beginning that the kinetic energy near the turning point can still be considered nonrelativistic. To identify the column density $N_{\rm max}$ where the assumption breaks down, we use Equation (13) with $\mathscr{E}_\perp^{\rm cr} = mc^2$, which gives the electric field $E_{\rm max}$ at that turning point. Substituting this to $E_{\rm max} = f_{\rm rel}(n/N_{\rm max})|\phi_{\rm max}|$, which follows from Equations (9) and (10), we obtain $e|\phi_{\rm max}| = (M_{\rm cr}/f_{\rm rel})\,N_{\rm max}L(mc^2)$. Next, we introduce the column density $N_* \approx 3\times 10^{22}$ cm^{-2} at which the electron extinction energy in Equation (4) is equal to mc^2. Combining the two equations, we derive

$$\frac{e|\phi_{\rm max}|}{mc^2} = \frac{M_{\rm cr}}{f_{\rm rel}(1+s)}\frac{N_{\rm max}}{N_*}. \tag{C7}$$

Finally, by virtue of Equations (9) and (C6) we write $e|\phi_{\rm max}|/mc^2 = \psi(N_{\rm max}/N_{\rm rel})^{f_{\rm rel}}$. Equating with Equation (C7)

gives

$$\frac{N_{\max}}{N_{\rm rel}} = \left(\frac{\psi f_{\rm rel}(1+s)}{M_{\rm cr}}\frac{N_*}{N_{\rm rel}}\right)^{\frac{1}{1-f_{\rm rel}}}. \quad \text{(C8)}$$

Note that $N_{\max}$ is comparable to, or larger than, N_*. For the conditions illustrated in Figure 1, $N_{\rm rel} \approx 3\times10^{21}\,{\rm cm}^{-2}$ ($2\times10^{21}\,{\rm cm}^{-2}$) for $a=1$ (2), resulting in $N_{\max}\approx 5\times10^{22}\,{\rm cm}^{-2}$ ($2\times10^{22}\,{\rm cm}^{-2}$). Thus, $N_{\max}\gg N_{\rm rel}$ and our assumption is well justified for molecular clouds.

Appendix D
Joule Heating

We calculate the ratio of Joule heating H_J, given by Equation (26), to regular gas heating $H_{\rm CR}$ by CRs, given by Equation (27). Substituting Equation (21) into (27), we obtain

$$H_{\rm CR} = 4\pi\eta B j_0 L_0 \mathscr{E}_0 n\left(\frac{e|\phi|}{\mathscr{E}_0}\right)^{-(a+s-1)}. \quad \text{(D1)}$$

Inserting $E = f|\phi|/z$ in Equation (26) and keeping in mind that $\mathscr{E}_0/L_0 = (1+s)N_0$, we can then write the ratio as

$$\frac{H_J}{H_{\rm CR}} = \frac{(1+s)f^2}{4\pi\eta B}\frac{\sigma n}{e^2 j_0 N_0}\left(\frac{N_0}{nz_0}\frac{z_0}{z}\right)^2\left(\frac{e|\phi|}{\mathscr{E}_0}\right)^{a+s+1}. \quad \text{(D2)}$$

Next, by virtue of Equations (4) and (18) this can be written as

$$\frac{H_J}{H_{\rm CR}} = Q\left(\frac{N_0}{nz_0}\right)^{\frac{s-1}{s}}\left(\frac{N}{N_0}\right)^{\frac{1+a+s}{1+s}}\left(\frac{z_0}{z}\right)^2\left(\frac{e|\phi|}{\mathscr{E}_{\rm ext}}\right)^{a+s+1}, \quad \text{(D3)}$$

where

$$Q = \frac{(1+s)^{2-\frac{1}{s}} f^{1-\frac{1}{s}} M_{\rm cr}^{\frac{1}{s}}}{4\eta a s B} \quad \text{(D4)}$$

is a function of a and s (for given η). Then, inserting $z_0/z = (e\phi/\mathscr{E}_0)^{-1/f}$ with f from Equation (17), we find

$$\frac{H_J}{H_{\rm CR}} = Q\left[\left(\frac{N_0}{nz_0}\right)\left(\frac{N}{N_0}\right)^{\frac{s(1+s-a)}{(1+s)^2}}\left(\frac{e|\phi|}{\mathscr{E}_{\rm ext}}\right)^{\frac{s(1+s-a)}{1+s}}\right]^{\frac{s-1}{s}}. \quad \text{(D5)}$$

We notice that, using Equation (19), the first two factors in the brackets can be expressed via $e|\phi|/\mathscr{E}_{\rm ext}$. This finally yields

$$\frac{H_J}{H_{\rm CR}} = Q\left(\frac{e|\phi|}{\mathscr{E}_{\rm ext}}\right)^{-\frac{1}{s}+s}. \quad \text{(D6)}$$

For parameters of Figure 1, Q varies between about 7 and 10 for $1\leqslant a\leqslant 2$.

ORCID iDs

Kedron Silsbee https://orcid.org/0000-0003-1572-0505
Alexei V. Ivlev https://orcid.org/0000-0002-1590-1018

References

Ainsworth, R. E., Scaife, A. M. M., Ray, T. P., et al. 2014, ApJL, 792, L18
Bian, N. H., Kontar, E. P., & Brown, J. C. 2010, A&A, 519, A114
Bisbas, T. G., Papadopoulos, P. P., & Viti, S. 2015, ApJ, 803, 37
Blandford, R. D., & Ostriker, J. P. 1978, ApJL, 221, L29
Braginskii, S. I. 1965, RvPP, 1, 205
Caselli, P., & Ceccarelli, C. 2012, A&ARv, 20, 56
Ceccarelli, C., Dominik, C., López-Sepulcre, A., et al. 2014, ApJL, 790, L1
Draine, B. T. 2011, Physics of the Interstellar and Intergalactic Medium (Princeton, NJ: Princeton Univ. Press)
Galli, D., Walmsley, M., & Gonçalves, J. 2002, A&A, 394, 275
Glassgold, A. E., Galli, D., & Padovani, M. 2012, ApJ, 756, 157
Indriolo, N., & McCall, B. J. 2012, ApJ, 745, 91
Ivlev, A. V., Dogiel, V. A., Chernyshov, D. O., et al. 2018, ApJ, 855, 23
Ivlev, A. V., Silsbee, K., Sipilä, O., & Caselli, P. 2019, ApJ, 884, 176
Keto, E., & Caselli, P. 2008, ApJ, 683, 238
Keto, E., Rawlings, J., & Caselli, P. 2014, MNRAS, 440, 2616
Klimushkin, D. Y., & Mager, P. N. 2014, Ap&SS, 350, 579
Kulsrud, R., & Pearce, W. P. 1969, ApJ, 156, 445
Le Petit, F., Ruaud, M., Bron, E., et al. 2016, A&A, 585, A105
McKee, C. F. 1989, ApJ, 345, 782
Morlino, G., & Gabici, S. 2015, MNRAS, 451, L100
Neufeld, D. A., & Wolfire, M. G. 2017, ApJ, 845, 163
Oka, T., Geballe, T. R., Goto, M., et al. 2019, ApJ, 883, 54
Padovani, M., Galli, D., & Glassgold, A. E. 2009, A&A, 501, 619
Padovani, M., Ivlev, A. V., Galli, D., et al. 2020, SSRv, 216, 29
Padovani, M., Ivlev, A. V., Galli, D., & Caselli, P. 2018, A&A, 614, A111
Park, J., Caprioli, D., & Spitkovsky, A. 2015, PhRvL, 114, 085003
Prasad, S. S., & Tarafdar, S. P. 1983, ApJ, 267, 603
Shu, F. H., Adams, F. C., & Lizano, S. 1987, ARA&A, 25, 23
Silsbee, K., & Ivlev, A. V. 2019, ApJ, 879, 14
Silsbee, K., Ivlev, A. V., Padovani, M., & Caselli, P. 2018, ApJ, 863, 188
Spitkovsky, A., Xu, R., & Tsiolis, V. 2019, AAS/HEAD Meeting, 17, 107.10
Spitzer, L. J., & Tomasko, M. G. 1968, ApJ, 152, 971
Stone, E. C., Cummings, A. C., Heikkila, B. C., & Lal, N. 2019, NatAs, 3, 1013
Yusef-Zadeh, F., Muno, M., Wardle, M., & Lis, D. C. 2007, ApJ, 656, 847
Zhao, B., Caselli, P., Li, Z.-Y., et al. 2016, MNRAS, 460, 2050
Zhao, B., Caselli, P., Li, Z.-Y., & Krasnopolsky, R. 2018, MNRAS, 473, 4868